Syntheses, structures and magnetic properties of a family of metal carboxylate polymers *via in situ* metal–ligand reactions of benzene-1,2,3-tricarboxylic acid†

Yan-Zhen Zheng, Yue-Biao Zhang, Ming-Liang Tong,* Wei Xue and Xiao-Ming Chen*

Received 10th September 2008, Accepted 6th November 2008
First published as an Advance Article on the web 13th January 2009
DOI: 10.1039/b815843f

Nine new coordination polymers: $[Cu_3(ipO)_2(pyz)_2]$ (**5**), $[Cu_3(ipO)_2(4\text{-phpy})(H_2O)_2]$ (**6**), $[Cu(ip)(4\text{-phpy})_2]$ (**7**), $[Cu_3(ipO)_2(H_2O)_2]$ (**8**), $[Co(phen)(ip)(H_2O)]$ (**9**), $[Co_3(1,2,3\text{-btc})_2(4,4'\text{-bpy})_2(H_2O)_2]\cdot 2H_2O$ (**10**), $[Ni(1,2,3\text{-btcH})(4,4'\text{-bpy})(H_2O)]\cdot H_2O$ (**11**), $[Cd_5(1,2,3\text{-btc})_2(1,2,3\text{-btcH})_2(4,4'\text{-bpy})_3(H_2O)_2]$ (**12**) and $(1,2,3\text{-btcH}_3)(4,4'\text{-bpy})$ (**13**) ($1,2,3\text{-btcH}_3$ = 1,2,3-benzenetricarboxylic acid, ipO = 2-hydroxyisophthalate, 4,4′-bpy = 4,4′-bipyridine, pyz = pyrazine, 4-phpy = 4-phenyl-pyridine and phen = *o*-phenanthroline) have been hydrothermally synthesized. This family of compounds show the role of the *N*-containing heterocyclic ligands and Cu(II) ions in the metal–ligand reactions. These results suggest that the hydroxylation requires Cu(II) ions as the oxidant, rather than the presence of *N*-containing heterocyclic ligands, while the decarboxylate procedure requires high temperature and basic condition rather than the participation of Cu(II) ions. The obtained compounds show versatile structures and magnetic properties due to the flexibility of the carboxylate ligands. Compound **5** shows dominated antiferromagnetic interaction in the $[Cu_2(\mu\text{-ipO})_2]$ unit, and no long-range magnetic ordering behaviour. Compound **10** has a topologically ferrimagnetic chain with alternating $Co^{II}_{oct}Co^{II}_{tet}Co^{II}_{oct}$ (oct = octahedral, tet = tetrahedal) spin arrangement. The Co^{II}_{tet} and Co^{II}_{oct} ions are bridged by similar *syn–anti* carboxylates ($Co^{II}_{tet}\cdots Co^{II}_{oct}$ 4.616 and 4.735 Å). Such a chain shows ferro- and antiferro- magnetic interactions and no long-range magnetic ordering behaviour was observed. Compound **11** has a antiferromagnetic coupled *syn–anti* carbxylate-bridged Ni(II) chain (J = 1.48(2) K), and shows long-range magnetic order below 2.6 K due to the extensive hydrogen bonds between the chains.

Introduction

Solvothermal (including hydrothermal hereafter) *in situ* metal–ligand reactions, as a new bridge between coordination chemistry and organic synthetic chemistry, has attracted intensive interest in recent years.[1] The research topics in this area are mainly focused on: (i) discovering new "one-pot" reaction avenues for some inaccessible or not easily accessible organic reactions at normal ambient conditions; (ii) applying the obtained ligands for generation of new functional coordination materials and (iii) clarifying the reaction mechanisms.

In the past decade, several interesting solvothermal *in situ* metal–ligand reactions, including dehydrogenative carbon–carbon coupling,[2] hydroxylation of aromatic rings,[3,4] cycloaddition of organic nitriles with azide and ammonia,[5] transformation of inorganic and organic sulfur,[6] as well as metal redox reactions have been discovered.[7] In some of the above reactions, the mechanisms of some reactions have been well explained by discovering the reaction intermediates, while others still remain unclear. Moreover, the application of these new ligands for designing new functional materials are in progress.[8]

Recently, we reported the *in situ* metal–ligand redox reaction of Cu^{II} and isophthalate (ip) yields $[Cu_2(ipO)(4,4'\text{-bpy})]$ (ipO = 2-hydroxyisophthalate, 4,4′-bpy = 4,4′-bipyridine) (**1**),[4a] and relevant reactions by using Cu(II) and 1,2,3-benzinetricarboxylic acid ($1,2,3\text{-btcH}_3$),[4b] which yielded **1**, $[Cu_3(ipO)_2(4,4'\text{-bpy})_{0.5}(H_2O)_2]$ (**2**), $[Cu_2(ip)(ipH)(4,4'\text{-bpy})_{1.5}]$ (**3**) and $[Cu_2(1,2,3\text{-btc})(4,4'\text{-bpy})(H_2O)_2](NO_3)$ (**4**), depending on the reaction pH conditions. Although we have already known that this reaction is highly related to the pH value, some questions, especially the role of Cu^{II} and 4,4′-bpy (hereafter using L-ligand to represent the *N*-containing heterocyclic and H_2O ligands in this reaction), still need to be answered.

Moreover, the carboxylate ligands as a mediator between the metal centers can transfer or separate the magnetic communications.[9] Therefore, some carboxylate ligands, especially those with multi-carboxylate ends at one side might be good candidates for creating low-dimensional magnetic compounds,[10] as exemplified by our incorporation of the Ising-type ferromagnetic Co^{II}-carboxylate chain into a two-dimensional (2D) network to form a new type of single-chain magnet.[10a,11]

Following our previous investigations[4a,b] on the *in situ* metal–ligand of Cu^{II} and ip, we present herein a systematic research on this reaction, which aims at on one hand, clarifying the role of

MOE Laboratory of Bioinorganic and Synthetic Chemistry, State Key Laboratory of Optoelectronic Materials and Technologies, School of Chemistry & Chemical Engineering, Sun Yat-Sen University, Guangzhou 510275, China. E-mail: tongml@mail.sysu.edu.cn, cxm@mail.sysu.edu.cn; Fax: +86 20 8411 2245; Tel: +86 20 8411 2074

† Electronic supplementary information (ESI) available: Crystal packing diagrams of **9**, **12** and **13**. CCDC reference numbers 701820–701828. For ESI and crystallographic data in CIF or other electronic format see DOI: 10.1039/b815843f

Cu^{II} and L and, on the other hand, obtaining low-dimensional magnetic compounds by this *in situ* formation method.

Results and discussion

Syntheses

All the reactions are summarized in Scheme 1, which shows that the analogous ligands of 4,4′-bpy, such as pyrazine (pyz) and 4-phenyl-pyridine (4-phpy), can also lead to the formation of hydroxylated products in the presence of Cu^{II}: $[Cu_3(ipO)_2(pyz)_2]$ (**5**), $[Cu_3(ipO)_2(4\text{-phpy})(H_2O)_2]$ (**6**) and a by-product [Cu(ip)(4-phpy)$_2$] (**7**). Even in the absence of an *N*-containing heterocyclic ligand, a hydroxylated product $[Cu_3(ipO)_2(H_2O)_2]$ (**8**) can also be formed, which suggests that the phenyl ring hydroxylation reaction can occur in the absence of any *N*-containing heterocyclic ligand. However, the yields of these hydroxylated products decrease in a sequence of 4,4′-bpy (95%) > pyz (45%) > H_2O (23%) ≈ 4-phpy (21%), implying that 4,4′-bpy can increase hydroxylation yield.

Other transition metal ions were also employed to examine the role of Cu^{II} ion in this *in situ* metal–ligand redox reaction. The results show that other metal ions, such as Co^{II}, Ni^{II}, Cd^{II}, Fe^{II} and Fe^{III}, can not induce the 1,2,3-btcH_3 ligand turn into a ipO ligand even at highly basic condition. If *o*-phenanthroline (phen) and Co^{II} ion were employed, a decarboxylate product [Co(phen)(ip)(H_2O)] (**9**) can be obtained under basic conditions. In contrast, the carboxylate products of $[Co_3(1,2,3\text{-btc})_2(4,4'\text{-bpy})_2(H_2O)_2]\cdot 2H_2O$ (**10**), [Ni(1,2,3-btcH)(4,4′-bpy)(H_2O)]·H_2O (**11**), $[Cd_5(1,2,3\text{-btc})_2(1,2,3\text{-btcH})_2(4,4'\text{-bpy})_3(H_2O)_2]$ (**12**) and (1,2,3-btcH_3)(4,4′-bpy) (**13**) can be obtained with very high yields at acidic condition. These results suggest that the hydroxylation requires Cu^{II} ions as the oxidant, while the decarboxylate procedure requires the high temperature and basic condition rather than the participation of Cu^{II} ions.

Possible mechanism of ipOH formation

Based on the above and previous results, the *in situ* metal–ligand reaction from 1,2,3-btc to ipO is suggested to be a two-step procedure containing decarboxylation and hydroxylation reactions, as shown in Scheme 2. Obviously, it is easy for 1,2,3-btc to decarboxylate at the 2-site position in the first step when heating it in basic condition, leading to the formation of ip. In the second step, the hydroxylation can be considered as a redox reaction of ip, which has been previously revealed.[4a] In this step, the carbon atom at the 2-position is a electron-poor site due to the electron withdrawing effect of adjacent carboxylate groups. Moreover, the coordination of Cu^{II} ions can enhance the electron

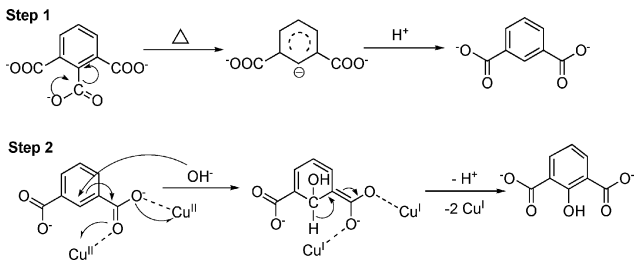

Scheme 2 A possible mechanism of the reaction between 1,2,3-btc and Cu^{II} in basic condition.

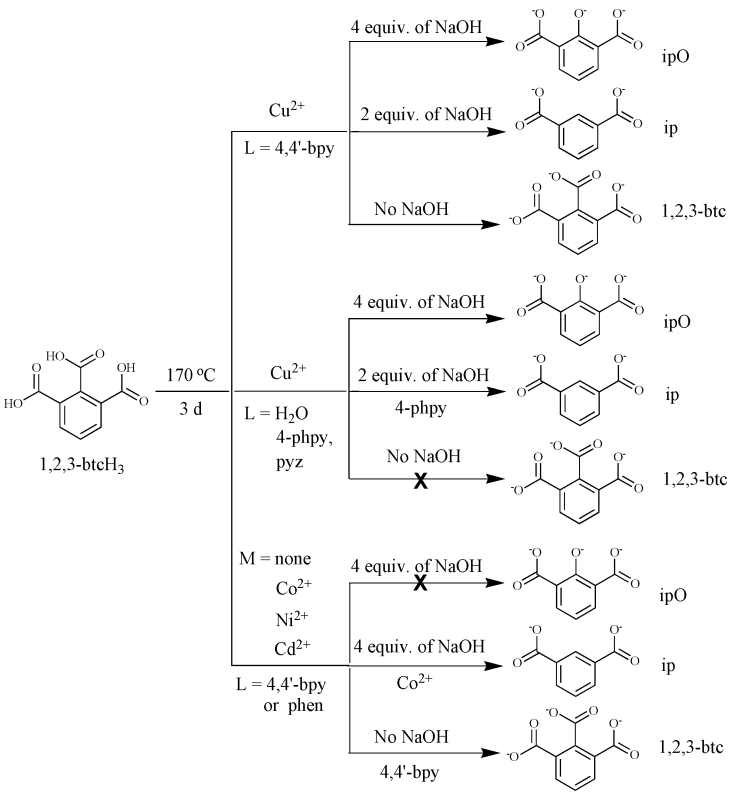

Scheme 1 The fate of 1,2,3-btcH_3 at different reaction conditions.

withdrawing effect, and cause the electron transfer from the ligand to Cu^{II} ions (two electrons are transferred and two Cu^{I} ions are produced when one ip is oxidized).[12] However, the Cu^{I} ions are not observed in **5**, **6** and **7**, which may be attributed to the formation of insoluble cuprous oxide and other soluble cuprous compounds. Actually, we did observe a small amount of unrecognized dark red (the color of cuprous oxide) powder admixtured with the products. This deduction is also supported by the fact that in the absence of Cu^{II} ions, no ipO containing product was isolated.

Crystal structures

$[Cu_3(ipO)_2(pyz)_2]$ (5). The asymmetric unit of **5** is a homodivalent Cu^{II} trimer, being similar to that of **2**, as shown in Fig. 1a. However, the crystallographically unique Cu2 is coordinated by the carboxylate oxygen atoms, rather than two aqua ligands in **2**. Therefore, the crystallographic symmetry of **5** is higher than that of **2**. It should be noted that the carboxylate ends of ipO exhibit two different coordination modes: one is the bidentate-bridging associated with Cu1 and Cu2 ions, the other is *anti–anti* bridging with two Cu1 ions. The pyz ligand also connects Cu2 ions, giving rise a 3D network (Fig. 1b) in **5** rather than the 2D layers in **2**, due to the different lengths of pyz and 4,4′-bpy, respectively.

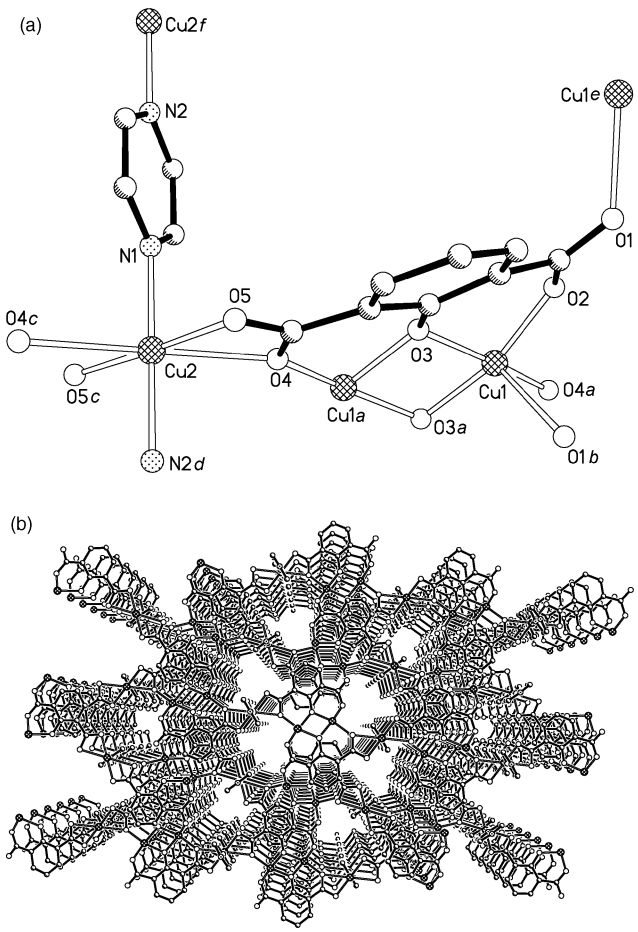

Fig. 1 The coordination environments (a) and 3D packing diagram (b) in **5**. Selected $Cu^{II}\cdots Cu^{II}$ distances (Å): $Cu(1)\cdots Cu(1)^{a}$ 2.981(1), $Cu(2)\cdots Cu(1)^{a}$ 4.143(1), $Cu(2)\cdots Cu(2)^{f}$ 6.827(1), $Cu(1)\cdots Cu(1)^{e}$ 5.955(1); and bond angles (°): $Cu(1)–O(3)–Cu(1)^{a}$ 100.53(14), $Cu(1)^{a}–O(4)–Cu(2)$ 149.6(2). Symmetry codes:[a] $-x, -y + 1, -z + 1$; [b] $x + 1/2, -y + 3/2, z$; [c] $x, -y + 1, -z + 3/2$; [d] $x + 1, y, z$; [e] $x - 1/2, -y + 3/2, z$; [f] $x - 1, y, z$.

$[Cu_3(ipO)_2(4\text{-phpy})(H_2O)_2]$ (6). The asymmetric unit of **6** is more similar to that of **2** than that of **5**, as shown in Fig. 2a, because the Cu3 ion is coordinated with two water molecules. The two carboxylate ends of ipO have similar coordination modes of **2** and **5**. Although the 4-phpy is a terminal ligand, the weakly coordinated carboxylate oxygen at the axial position of the Cu^{II} square-pyramid links the $[Cu_2^{II}(ipO)_2Cu^{II}]$ chain into a stairs-like layer (Fig. 2b). There are also extensive hydrogen bonding interactions in the lattice due to presence of the aqua ligands.

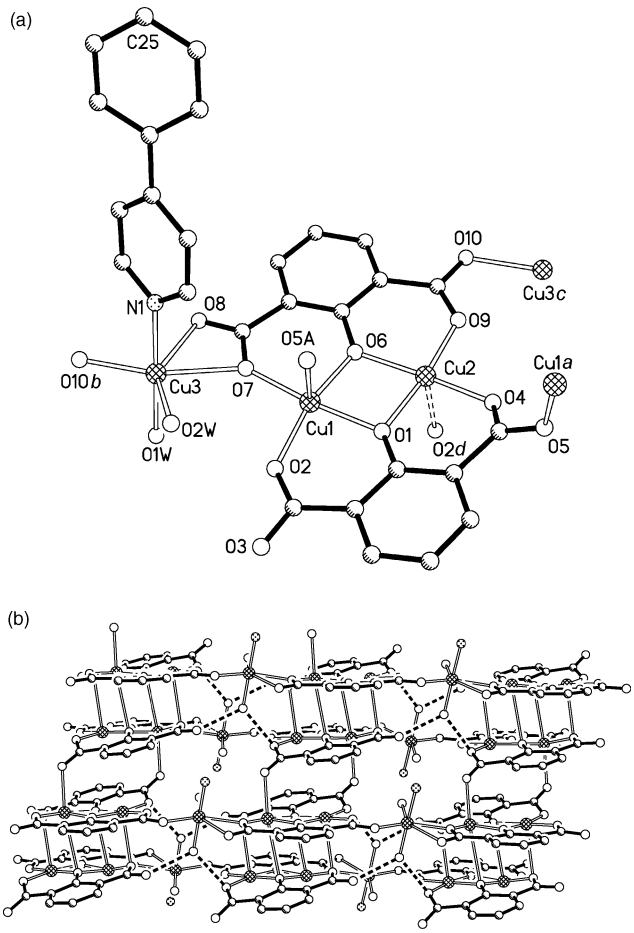

Fig. 2 The coordination environments (a) and 2D packing diagram (omitting the rings of 4-phpy for clarity) (b) in **6**. Selected $Cu^{II}\cdots Cu^{II}$ distances (Å): $Cu(1)\cdots Cu(2)$ 2.9443(7), $Cu(1)\cdots Cu(3)$ 3.854(3), $Cu(1)\cdots Cu(2)^{d}$ 3.547(3), $Cu(1)\cdots Cu(2)^{a}$ 5.479(3); and angles (°): Cu(1)–O(1)–Cu(2) 100.7(1), Cu(2)–O(6)–Cu(1) 100.0(1), Cu(1)–O(7)–Cu(3) 136.3(1)°. Symmetry codes: [a] $-x + 1, -y, -z + 1$; [b] $x, y, z - 1$, [c] $x, y, z + 1$; [d] $-x + 2, -y, -z + 1$.

$[Cu(ip)(4\text{-phpy})_2]$ (7). The structure of **7** features a 2D layer constructed by Cu^{II}-ip chains and the 4,4′-bpy pillars (Fig. 3). The coordination modes of the ip carboxylate ends in **7** are also different: one is a *syn–syn* bridging mode with the inversely-related Cu^{II} dimer ($Cu^{II}\cdots Cu^{II}$ 4.509 Å), the other is virtually a bidentate-chelating mode, since the two Cu–O bonds are very different (Cu1–O1 1.978(4) and Cu1–O2 2.714 Å). Therefore, this

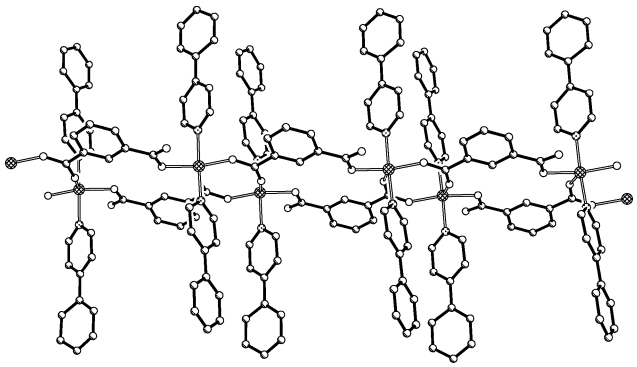

Fig. 3 The layered structure in **7**.

bidentate-chelating mode can be also be treated as monodentate, as shown in Fig. 3.

[$Cu_3(ipO)_2(H_2O)_2$] (8). The structure of **8** has been reported in the literature, and we will not repeat here.[13]

[Co(phen)(ip)(H_2O)] (9). The structure of **9** features a simple 1D Co^{II}-ip chain (Fig. 4), in which the Co^{II} ion is six-coordinated by three carboxylate-*O* atoms (Co–O 2.030(2)-2.195(5) Å), one aqua ligand (Co–O 2.110(2) Å) and two nitrogen atoms from the phen ligand (Co–N 2.095(2)–2.121(2) Å). The μ-ip ligand also has two coordination modes: chelating and monodentate, which are different from those in **7**. These chains are further stacked *via* π–π stacking interactions of the phen rings and hydrogen bonds between the aqua ligand and carboxylate groups (Fig. S1).†

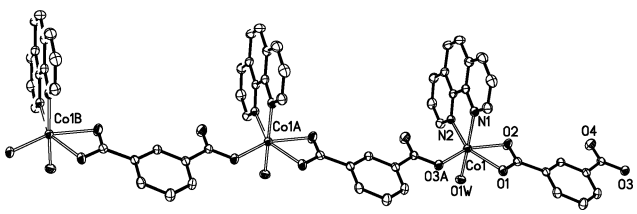

Fig. 4 ORTEP view (35% possibility) of the 1D chain in **9**.

[Co_3(1,2,3-btc)$_2$(4,4′-bpy)$_2$(H_2O)$_2$]·2H_2O (10). The asymmetric unit of **10** has one and a half Co^{II} ions in different coordination geometries (Fig. 5a). Co1 is six-coodinated by three oxygen atoms from three carboxylate groups (Co–O 2.063(5)–2.084(6) Å) and one aqua ligand (Co–O 2.185(6) Å), and two nitrogen atoms from two different 4,4′-bpy ligands (Co–N 2.110(6)-2.146(7) Å). Co2 is four-coordinated by four oxygen atoms from four carboxylate groups (Co–O 1.975(6)–1.979(6) Å). The Co1 and Co2 ions are bridged by four *syn–anti* carboxylate groups to form an alternating chain ($Co^{II}\cdots Co^{II}$ 4.616–4.735 Å) (Fig. 5b). Such chains are extended along the *c* direction, and connected by the 4,4′-bpy ligands to form a 3D networks (Fig. 5c). The guest water molecules occupy 14.4% void space of the crystal volume.

[Ni(1,2,3-btcH)(4,4′-bpy)(H_2O)]·H_2O (11). There is only one six-coordinated Ni^{II} ion with four planar oxygen atoms from the carboxylate groups (Ni–O 2.038(2)–2.106(1) Å) and two axial nitrogen atoms from the 4,4′-bpy (Ni–N 2.090(2)–2.111(2) Å) in the asymmetric unit (Fig. 6a). Therefore, the 1,2,3-btcH_3 is not fully deprotonated for the charge balance. One of the three

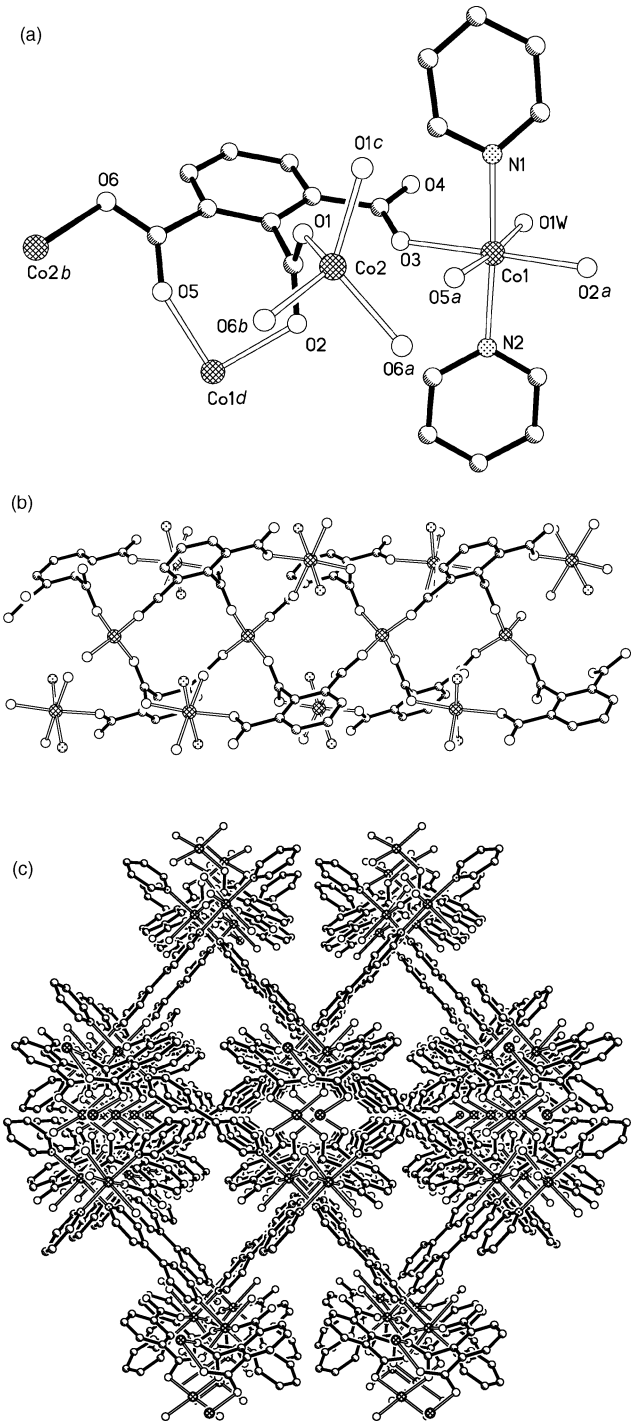

Fig. 5 The coordination environments (a), 1D Co^{II}-carboxylate chain along the *c* axis (b) and a packing diagram along the *c* axis (c) in **10**. Symmetry codes: [a] *x*, −*y* + 1, *z* − 1/2; [b] −*x* + 1, −*y* + 1, −*z*; [c] −*x* + 1, *y*, −*z* − 1/2; [d] *x*, −*y* + 1, *z* + 1/2.

carboxylate groups adopts a *syn–anti* bridging mode to connect another Ni^{II} ion with a $Ni^{II}\cdots Ni^{II}$ separation of 5.160 Å (Fig. 6b). The Ni^{II}-carboxylate chains are further assembled into a 2D layer by the 4,4′-bpy bridges (Fig. 6c). Such layers are further connected with the hydrogen bonds between the protonated carboxylate ends.

[Cd_5(1,2,3-btc)$_2$(1,2,3-btcH)$_2$(4,4′-bpy)$_3$(H_2O)$_2$] (12). The asymmetric unit of **12** has two and a half Cd^{II} atoms, one

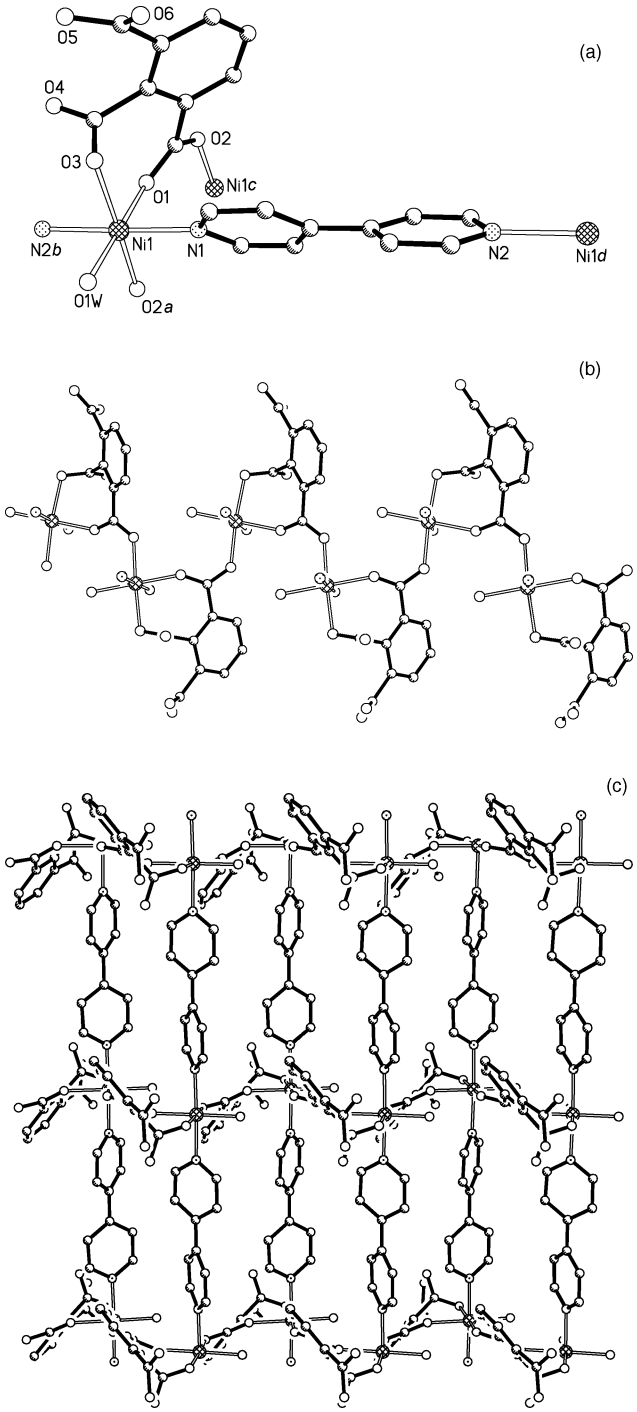

Fig. 6 The coordination environments (a), Ni(II)-carboxylate chain (b) and the 4,4′-bpy-pillared layer (c) in **11**. Symmetry codes: [a] $-x + 5/2$, $y + 1/2$, $-z + 5/2$; [b] $x - 1$, y, z; [c] $-x + 5/2$, $y - 1/2$, $-z + 5/2$; [d] $x + 1$, y, z.

deprotonated 1,2,3,-btc, and one protonated 1,2,3-btcH, one and a half 4,4′-bpy and one aqua ligands (Fig. 7). Cd1 and Cd3 are six-coordinated, while Cd2 is seven-coordinated. The Cd–O and Cd–N bond lengths are in the normal range of 2.243(5)–2.571(6) and 2.276(6)–2.372(6) Å, respectively. The 1,2,3-btc and 1,2,3-btcH ligands connect the Cd^{II} ions into a 2D layer in the *ab* plane, and the 4,4′-bpy pillar the layers into a 3D network (Fig. S2).†

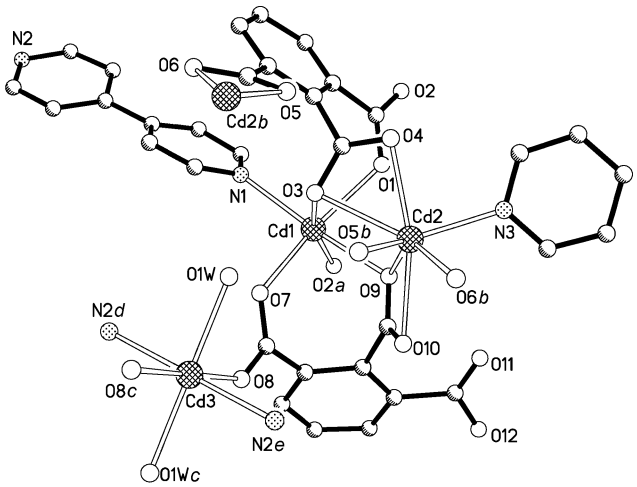

Fig. 7 The coordination environments in **12**. Symmetry codes: [a] $-x + 1$, $-y$, $-z - 2$; [b] $-x + 1$, $-y + 1$, $-z - 2$; [c] $-x$, $-y + 1$, $-z - 2$; [d] $-x$, $-y$, $-z - 3$; [e] x, $y + 1$, $z + 1$.

$(1,2,3\text{-btcH}_3)(4,4'\text{-bpy})$ (13). The structure of **13** is a typical hydrogen bonded network constructed by hydrogen bonding interactions between the carboxylate groups and the nitrogen atoms of the 4,4′-bpy (Fig. 8 and Fig. S3).† The high yield of **13** suggests that hydrogen bonding may be helpful to stabilize the carboxylate at the 2-position of 1,2,3-btc.

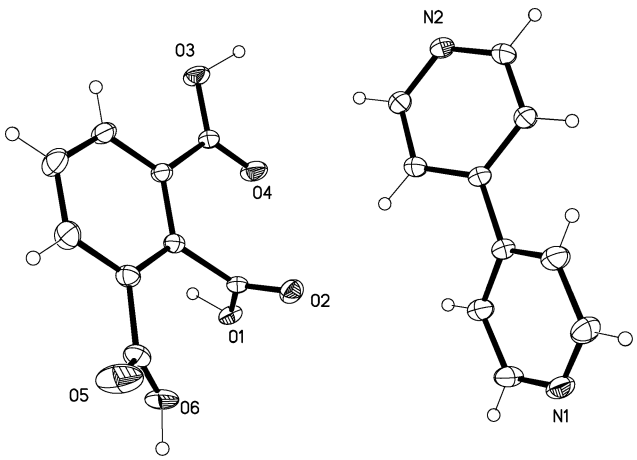

Fig. 8 ORTEP view (30% possibility) of the asymmetric unit of **13**.

Magnetic properties

Magnetic properties of 5. The temperature-dependent susceptibility data of **5** has been measured under a dc field of 5 KOe (Fig. 9). At 300 K, the χT value is 0.77 $cm^3mol^{-1}K$, significantly lower than the expected value of 1.13 $cm^3mol^{-1}K$ for non-coupled Cu^{II}_3 unit, indicating dominated antiferromagnetic coupling between the magnetic centres. Upon cooling, the χT plot decreases smoothly and then reach a platform below 100 K, the χT value is close 0.42 $cm^3mol^{-1}K$, a value that is close to a net magnetic moment for spin of 1/2 (0.38 $cm^3mol^{-1}K$). Below 20 K, the χT plot drops quickly, which is caused by the antiferromagnetic interactions between the Cu^{II} trimers.[14] At 2.0 K, the field-dependent magnetization was increasing linearly

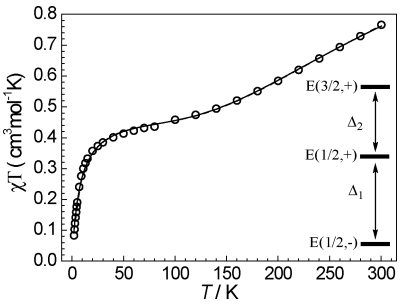

Fig. 9 Temperature-dependent susceptibility data of **5** under a dc field of 5 KOe. Solid and dashed lines: fitting results of eqn (2) and eqn (4), respectively.

to a maximum value of 0.48 $N\beta$ (Fig. 10), indicating the magnetic moment is still unsaturated (the expected saturated value is $M_s = nSg = 1\ N\beta$). This behaviour is probably due to the significant antiferromagnetic interactions between the Cu^{II} ions since the Cu^{II} ions are not so anisotropic.

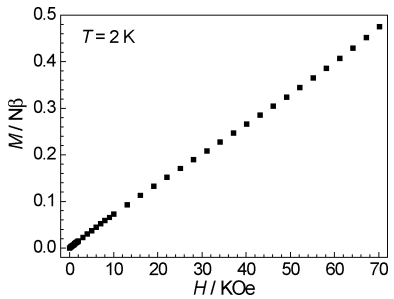

Fig. 10 Field-dependent magnetization of **5** at 2 K.

To further study the magnetic behaviour of **5**, we used the following Heisenberg Hamiltonian, eqn (1) since it has the basic magnetic unit of $[Cu_2(\mu\text{-ipO})_2Cu]$ (Fig. 11),

$$\hat{H} = -2(J_{12}\hat{S}_1\hat{S}_2 + J_{13}\hat{S}_1\hat{S}_3 + J_{23}\hat{S}_2\hat{S}_3) \quad (1)$$

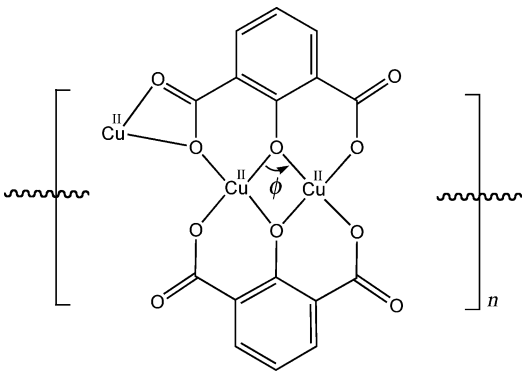

Fig. 11 The repeating $[Cu_2(\mu\text{-ipO})_2Cu]$ unit in **5**.

which gives two spin doublet and one spin quartet states with the following respective energies: $E(3/2) = -(2J_{12} + 2J_{13} + 2J_{23})/4$ and $E(1/2,\pm) = (2J_{12} + 2J_{13} + 2J_{23})/4 \pm \{[(2J_{12} - 2J_{13})^2 + (2J_{23} - 2J_{12})^2 + (2J_{13} - 2J_{23})^2]/8\}^{1/2}$. The resulting analytical expression is:

$$\chi = \frac{Ng^2\beta^2}{k_B(T-\theta)} \frac{0.5 + 0.5\exp(\Delta_1/k_BT) + 5\exp(-\Delta_2/k_BT)}{2 + 2\exp(\Delta_1/k_BT) + 4\exp(-\Delta_2/k_BT)} \quad (2)$$

where $\Delta_1 = E(1/2,+) - E(1/2,-)$, and $\Delta_2 = E(3/2,+) - E(1/2,+)$, as shown in Fig. 10. Taking into account the trimeric units in **5** are highly correlated, a mean field approximation (θ) was employed. Fitting eqn (2) gives $\Delta_1 = 286\ cm^{-1}$, $\Delta_2 = 165\ cm^{-1}$, $g = 2.27$ and $\theta = -7.7$ K. The fact that the quartet is far above the ground state may indicates that all the J_{ij} values are antiferromagnetic. The large zJ' value indicates that antiferromagnetic interactions between the trimer are significant, which is reasonable because all the trimers are linked by carboxylate bridges.

An arising problem is no way to determine three independent J_{ij} values unambiguously by only Δ_1 and Δ_2. As demonstrated by Gatteschi *et al.*,[15] the the J_{ij} values can only be estimated in a certain range by the above model.

To simplify the model, the Hamiltonian can be written as:

$$\hat{H} = -2J(\hat{S}_1\hat{S}_2 + \hat{S}_2\hat{S}_3) \quad (3)$$

which neglects the difference of J_{12} and J_{23}, and also omits J_{13}. This Hamiltonian leads to the following equation.

$$\chi T = \frac{Ng^2\beta^2}{4k_B} \frac{1 + \exp(J/k_BT) + 10\exp(3J/2k_BT)}{1 + \exp(J/k_BT) + 2\exp(3J/2k_BT)} \quad (4)$$

Unexpectedly, a very good simulation of the χT plot, and the obtained parameters are shown in Table 1. The large negative J value indicates strong antiferromagnetic interaction in the $Cu_2(\mu\text{-ipO})_2$ dimer is dominated in this trimer, and the antiferromagnetic interaction between the $Cu_2(\mu\text{-ipO})$ dimer and the single Cu^{II} ion is much weaker.

Since the $Cu^{II}_2(\mu\text{-OR})_2$ dimers have been widely studied, and the factors influencing the strength of superexchange—couplings are mainly associated with ϕ.[16] We used the famous, empirical analytical expression: eqn (5),

$$J(cm^{-1}) = 74\phi + 7270 \quad (5)$$

to test our results. Surprisingly, we found that the value obtained by eqn (5) is closer to the value calculated from eqn (4), which may indicate that the antiferromagnetic interactions in the trimeric $[Cu_2(\mu\text{-ipO})_2Cu]$ unit are almost attributed to the $Cu_2(\mu\text{-OR})_2$ part.

Magnetic properties of 10. The temperature-dependent susceptibility data of **10** were measured under a dc field of 1.0 KOe (Fig. 12). At room temperature (300 K), the χT value is 9.69 $cm^3mol^{-1}K$, which is significantly larger than the expected spin-only value (5.63 $cm^3mol^{-1}K$) for three non-coupled Co^{II} ions, indicating that the orbital contribution of the octahedral Co^{II} ions

Table 1 Magnetic fitting results with different models of **5**

eqn (2)				eqn (4)			eqn (5)	
Δ_1/cm^{-1}	Δ_2/cm^{-1}	zJ/cm^{-1}	g	J/cm^{-1}	zJ'/cm^{-1}	g	$\phi/°$	J/cm^{-1}
286	165	−7.7	2.27	−149	−10.7	2.27	100.5	−167

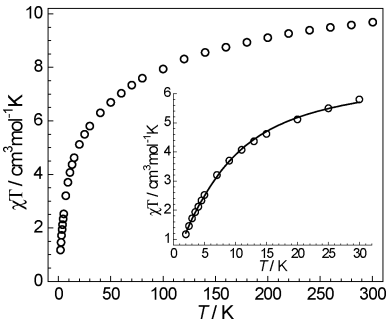

Fig. 12 Temperature-dependent susceptibility data of **10** under a dc field of 1 KOe. Inset: enlargement of the data below 30 K. Solid line: fitting result of eqn (6).

in **10** is significant.[14] If converting this orbital contribution to the g value, one gets a g value of 2.63 for **10**, which is large, but still normal for an octahedral Co^{II} compound. Upon cooling, the χT plot decreases smoothly down to 50 K. In this region, the susceptibility data were well fitted by the Curie–Weiss law, $\chi = C/(T - \theta)$, which gives a C value of 10.59 $cm^3mol^{-1}K$ and a θ value of −31.83 K. The moderate negative θ value may indicate not only the spin–orbital coupling of the single Co^{II} ion, but also antiferromagnetic coupling effect between the Co^{II} ions. Below 30 K, the χT plot drops quickly, which may be caused by the zero-field splitting effect and/or antiferromagnetic interaction of the Co^{II} ions.[12] At 2.5 K, the field-dependent magnetization was increasing to a maximum value of 5.94 $N\beta$ (Fig. 13), indicating the magnetic moment is still unsaturated. This behaviour is typically the octahedral Co^{II} ion with significant single-ion anisotropy and the effective spin-1/2 below 30 K.[14]

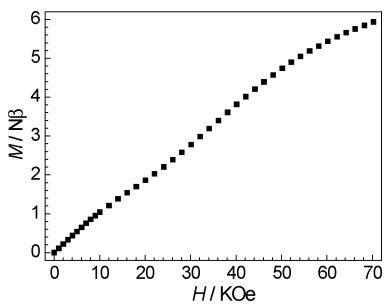

Fig. 13 Field-dependent magnetization of **10** at 2.5 K.

As mentioned in the structural description above, **10** features a topologically ferrimagnetic Co^{II}-carboxylate chain (Scheme 3), which is further connected by the 4,4′-bpy ligand. Therefore, these spin-chains in **10** are well isolated. Because the distances between the octahedral Co1 and tetrahedral Co2 ions are slightly different, we use two J to describe the coupling pathways in this chain.

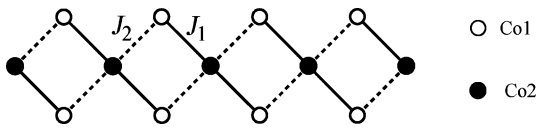

Scheme 3 The spin-coupling pathways of the topological ferromagnetic chain in **10**.

This kind of topological-ferrimagnetic spin-1/2 chain has been studied by Drillon *et. al.* with the following Hamiltonain: eqn (6),[17]

$$\hat{H} = -J_1\sum(\hat{S}_{3n-1}\hat{S}_{3n} + \hat{S}_{3n}\hat{S}_{3n+1}) - J_2\sum(\hat{S}_{3n}\hat{S}_{3n+2} + \hat{S}_{3n+1}\hat{S}_{3n+3}) - g_BH(\hat{S}_{3n} + \hat{S}_{3n-1} + \hat{S}_{3n+1}) \quad (6)$$

which treats the chain as interacting linear trimers. We applied this analytical expression[17] to fit the magnetic data of **10** from 30–2 K, which gives $J_1 = -17.7(4)$ K, $J_2 = 1.38(6)$ K and $g = 4.95(3)$. The large g value is consistent with the treatment of effective spin 1/2 for Co^{II} ions below 30 K. The obtained J values indicate both ferro- and antiferro-magnetic interactions coexist in the *syn–anti* carboxylate-bridged Co^{II} ions, which are also observed in other metal ions.[7b,18] However, the lack of onset of the χT plot does not imply the ferrimagnet-like behaviour in **10**. According to eqn (6), such a topologically ferrimagnetic chain behaves as an antiferromagnetic chain when $|2J_1| > J_2$, which is in accordance with the fitting result.[17b]

Magnetic properties of 11. The temperature-dependent susceptibility data of **11** were measured under a dc field of 1 KOe (Fig. 14). At room temperature (305 K), the χT value is 1.24 $cm^3mol^{-1}K$, which is larger than the expected spin-only value (1.00 $cm^3mol^{-1}K$) for a one non-coupled Ni^{II} ion, and consistent with other compounds with an octahedral Ni^{II} ion.[14] Upon cooling, the χT plot decreases gradually down to 50 K. In this region, the susceptibility data were well fitted by the Curie–Weiss law with a C value of 1.19 $cm^3mol^{-1}K$ and a θ value of 6.11 K. The small positive θ value may indicate the ferromagnetic coupling between the Ni^{II} ions. This conclusion is further supported by the χT plot below 50 K, which shows a quick increase before goes to the maximum of 2.50 $cm^3mol^{-1}K$ at 2.6 K. The presence of the maximum in the χT plot may indicate a long-range magnetic ordering behaviour in **11**. The susceptibility data from 300–6 K can be well simulated by the Fisher model, eqn (7):[19]

$$\chi_{chian} = \frac{N(M\beta)^2}{3k_BT}\frac{(1-u)}{(1+u)} \quad (7)$$

where $M = g[S(S+1)]^{1/2}$ and $u = \coth(J/k_BT) - k_BT/J$. In order to fit experimental data, the exchange energy J must be scaled following the usual procedure: $J \rightarrow JS(S+1)$. The best fitting gives $J = 1.48(2)$ K and $g = 2.215(3)$. The positive J value shows weak ferromagnetic interactions in the *syn–anti* carboxylate-bridged Ni^{II} chain, which was also observed in some known examples.[7b,18]

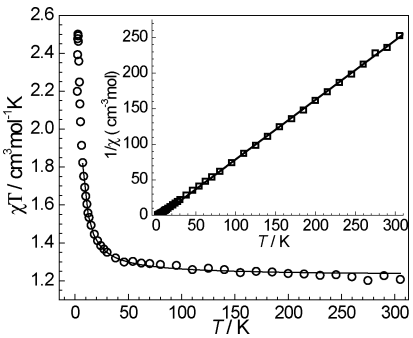

Fig. 14 Temperature-dependent susceptibility data of **11** under a dc field of 1KOe. Solid line: fitting result of eqn (7). Inset: the temperature dependent inverse molecular susceptibility. Solid line: fitting result of Curie–Weiss law.

The field-dependent magnetization at 2 K shows a maximum value of 2.0 $N\beta$ (Fig. 15) at 70 kOe, indicating the magnetic moment is almost saturated (the expected saturated value $Ms = nSg = 2\ N\beta$, assuming $g = 2$). To confirm the ferromagnetic interactions between the Ni^{II} ions, we plotted the Brillouin curve for uncoupled spin 1, which is below the M–H plot of **11** when the field is less than 30 kOe. This behaviour indicates a system with ferromagnetic interaction.[14]

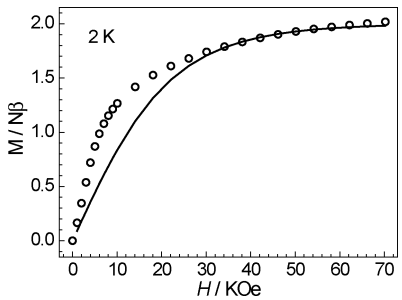

Fig. 15 Field-dependent magnetization of **11** at 2 K. Solid line: the simulated Brillouin function with $S = 1$.

Hysteresis loop of **11** was also observed at 1.8 K (Fig. 16). Small coercive field (10 kOe) was observed from the magnified curve, which indicates an irreversible effect below the Curie temperature. It should be noted that the "step" in the origin region of the hysteresis loop is caused by the inter-chain magnetic interaction,[20] which could be estimated from eqn (8):[21]

$$g\beta H_c S = 2|zJ'|S^2 \quad (8)$$

where H_c is the critical field that can be obtained from the maximum (2.2 kOe) of dM/dH plot. The obtained value of $|zJ'|$ is 0.17 K. Assuming $z = 2$, one gets $|J'| = 0.085$ K.

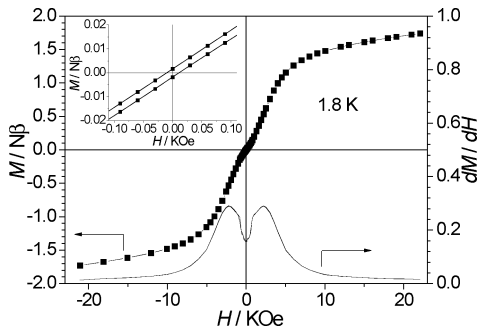

Fig. 16 Hysteresis loop of **11** at 1.8 K. Inset: the magnified region in the field range of ± 0.1 kOe (up) and the dM/dH plot (right).

After obtaining the $|J'|$ value, we can use it to estimate the T_c value by eqn (9):[22]

$$k_B T_C = 4S(S+1)|JJ'|^{1/2} \quad (9)$$

giving $T_c = 2.8$ K, which is in excellent agreement with the maximum of the χT plot at 2.6 K. The occurrence of long-range magnetic ordering behaviour of **11** would be attributed to the extensive hydrogen bonding interactions between the Ni^{II}-carboxylate chains.

Conclusions

In summary, we have successfully isolated nine new compounds *via* the *in situ* metal–ligand hydrothermal reaction of benzene-1,2,3-tricarboxylic acid. The results show that the decarboxylate reaction requires a high temperature and basic condition rather than the participation of Cu^{II} ions, while the hydroxylation requires Cu^{II} ions as the oxidant.

The resultant products show versatile structures and magnetic properties due to the flexibility of the carboxylate ligands. Although the similar *syn–anti* carboxylates bridge the Co^{II} (**10**) and Ni^{II} (**11**) ions, the magnetic interactions can be antiferro or ferromagnetic. Moreover, even the metal–carboxylate chains are assembled into high-dimensional network, the Co^{II} compound (**10**) does not undergo 3D long-range magnetic order, while the Ni^{II} compound (**11**) does. These results may indicate the "polymerization" method[7b,10] is feasible in assembling low-dimensional magnets, but hydrogen bonding interactions between the chains should be largely avoided.

Experimental

General procedures

Commercially available reagents have been used as received without further purification. The C, H and N microanalyses have been carried out with an Elementar Vario-EL CHNS elemental analyzer. The FT-IR spectra have been recorded from KBr pellets in the range 4000–400 cm^{-1} on a Bio-Rad FTS-7 spectrometer.

Synthetic procedures

$[Cu_3(ipO)_2(pyz)_2]$ (5). A mixture of $Cu(NO_3)_2{\cdot}3H_2O$ (0.242 g, 1.0 mmol), 1,2,3-$btcH_3{\cdot}2H_2O$ (0.123 g, 0.5 mmol), pyz (0.020 g, 0.25 mmol), water (10 cm^3) and NaOH (0.080 g, 2.0 mmol) in a 23-cm^3 autoclave with autogenerated pressure at 170 °C for 3 d, dark-blue block crystals were filtrated and washed by deionized water and ethanol (yield 45% based on pyz). Anal. calcd $C_{20}H_{10}Cu_3N_2O_{10}$: C 38.19, H 1.60, N 4.45. Found: C 38.08, H 1.57, N 4.48%. FT-IR data ν/cm^{-1}: 3420 m, 3105 w, 3041 w, 1600 vs, 1535 s, 1474 w, 1426 s, 1354 s, 1280 m, 1215 w, 1104 w, 1071 w, 874 w, 823 m, 756 m, 722 w, 640 m, 479 w.

$[Cu_3(ipO)_2(4\text{-phpy})(H_2O)_2]$ (6) and $[Cu(ip)(4\text{-phpy})_2]$ (7). Except the pyz was replaced by 4-phpy, a similar synthetic procedure of **5** was applied. Green block crystals of **6** were manually isolated from a small amount of green plate crystals of **7** (yield **6**, 21%; **7**, *ca.* 5%). Anal. calcd for **6**, $C_{27}H_{19}Cu_3NO_{12}$: C 43.82, H 2.59, N 1.89. Found: C 43.91, H 2.57, N 1.91%. For **7**, $C_{30}H_{22}CuN_2O_4$: C 66.95, H 4.15, N 5.20. Found: C 66.97, H 4.12, N 5.21%. FT-IR data ν/cm^{-1} for **6**: 3412 s, 3317 m, 3154 m, 1612 s, 1545 s, 1454 s, 1395 vs, 1293 w, 1050 m, 940 w, 881 w, 821 w, 771 m, 721 m, 623 w, 578, 525 w, 483 w. For **7**: 3378 m, 3072 w, 1603 vs, 1560 s, 1480 m, 1375 s, 1215 w, 1070 w, 819 m, 798 m, 734 m, 633 w, 475 w.

$[Cu_3(ipO)_2(H_2O)_2]$ (8). A same synthetic procedure as **5** was used without L to obtain the green block crystals of **8** (yield 23% based on 1,2,3-$btcH_3$). Anal. calcd $C_{16}H_{10}Cu_3O_{12}$: C 32.86, H 1.72. Found: C 32.66, H 1.75%. FT-IR data ν/cm^{-1}: 3410 s, 3319 m, 3150 m, 1613 s, 1548 vs, 1456 s, 1396 vs, 1288 m, 1051 m, 881 w, 769 m, 720 s, 619 w, 525 w, 482 w.

[Co(phen)(ip)(H_2O)] (9). A mixture of $Co(NO_3)_2{\cdot}3H_2O$ (0.291 g, 1.0 mmol), 1,2,3-btc$H_3{\cdot}2H_2O$ (0.123 g, 0.5 mmol), phen (0.100 g, 0.5 mmol), NaOH (0.080 g, 2.0 mmol) and water (10 cm^3) in a 23 cm^3 autoclave with autogenerated pressure at 170 °C for 3 d gave red block crystals of **9** (yield 95% based on 1,2,3-btcH_3). Anal. calcd $C_{20}H_{14}CoN_2O_5$: C 57.02, H 3.35, N 6.65. Found: C 57.06, H 3.34, N 6.60%. FT-IR data ν/cm^{-1}: 3162 m, 2143 w, 1636 s, 1612 s, 1565 s, 1465 m, 1450 s, 1395 s, 1158 m, 780 m, 758 m, 735 w, 585 w.

[Co_3(1,2,3-btc)$_2$(4,4′-bpy)$_2$(H_2O)$_2$]·2H_2O (10). A mixture of $Co(NO_3)_2{\cdot}6H_2O$ (0.291 g, 1.0 mmol), 1,2,3-btc$H_3{\cdot}2H_2O$ (0.123 g, 0.5 mmol), 4,4′-bpy (0.078 g, 0.5 mmol) and water (10 cm^3) was sealed in a 23 cm^3 autoclave with autogenerated pressure at 170 °C for 3 d yielding purple prism crystals of **10** (yield 93% based on 1,2,3-btcH_3), Anal. calcd $C_{38}H_{30}Co_3N_4O_{16}$: C 46.79, H 3.10, N 5.74. Found: C 47.81, H 3.07, N 5.71%. FT-IR data ν/cm^{-1}: 3411 br, 3315 m, 3150 m, 1611 s, 1544 s, 1450 s, 1394 vs, 1290 w, 1051 m, 944 w, 882 w, 819 w, 769 m, 711 m, 622 w, 528, 473 w.

[Ni(1,2,3-btcH)(4,4′-bpy)(H_2O)]·H_2O (11). By replacing $Co(NO_3)_2{\cdot}6H_2O$ with $Ni(NO_3){\cdot}6H_2O$ (0.291 g, 1.0 mmol), a similar synthetic procedure of **10** was used to obtained the green prism crystals of **11** (yield 91% based on 1,2,3-btcH_3), Anal. calcd $C_{19}H_{16}N_2NiO_8$: C 49.71, H 3.51, N 6.10. Found: C 49.68, H 3.52, N 6.11%. FT-IR data ν/cm^{-1}: 3410 br, 3312 m, 3152 m, 1605 s, 1540 s, 1445 s, 1391 vs, 1280 w, 1064 m, 940 w, 878 w, 818 w, 770 m, 719 m, 620 w, 525, 467 w.

[Cd_5(1,2,3-btc)$_2$(1,2,3-btcH)$_2$(4,4′-bpy)$_3$(H_2O)$_2$] (12). By replacing $Co(NO_3)_2{\cdot}6H_2O$ with $Cd(NO_3){\cdot}4H_2O$ (0.308 g, 1.0 mmol), a similar synthetic procedure of **10** was used to obtained the pale-yellow block crystals of **12** (yield 95% based on 1,2,3-btcH_3), Anal. calcd $C_{66}H_{42}Cd_5N_6O_{26}$: C 41.78, H 2.23, N 4.43. Found: C 41.75, H 2.25, N 4.41%. FT-IR data ν/cm^{-1}: 3411 br, 3310 m, 3151 m, 1600 s, 1545 s, 1444 s, 1390 vs, 1278 w, 1068 m, 942 w, 881 w, 819 w, 779 m, 722 m, 625 w, 528, 469 w.

(1,2,3-btcH_3)(4,4′-bpy) (13). A mixture of 1,2,3-btc$H_3{\cdot}2H_2O$ (0.123 g, 0.5 mmol), 4,4′-bpy (0.078 g, 0.5 mmol) and water (10 cm^3) was sealed in a 23 cm^3 autoclave with autogenerated pressure at 170 °C for 3 d yielding colourless block crystals of **13** (yield 96% based on 1,2,3-btcH_3), Anal. calcd $C_{19}H_{13}N_2O_6$: C 62.47, H 3.59, N 7.67. Found: C 62.45, H 3.58, N 7.65%. FT-IR data ν/cm^{-1}: 3089 br, 3001 br, 2880 br, 2664 br, 2549 br, 1691 vs, 1609 s, 1579 m, 1419 s, 1279 vs, 1161 m, 1075 w, 998 w, 931 m, 729 s, 689 s, 537 m.

Crystallographic structure determinations

Single-crystal X-ray diffraction intensities of **5–11** and **13** have been collected on a Bruker Apex CCD area-detector diffractometer by using MoKα ($\lambda = 0.71073$ Å) radiation. Absorption corrections have been applied by using the multi-scan program SADABS.[23] Diffraction intensities of **12** were collected on a Siemens R3 diffractometer using the ω-scan technique. Lorentz-polarization and absorption corrections were applied.[24] All the structures were solved with direct methods and refined with a full-matrix least-squares technique with the SHELXTL program package.[25] Anisotropic thermal parameters have been assigned to all non-hydrogen atoms. The organic-ligand bound hydrogen

Table 2 Crystal and structure refinement for **5–13**

	5	**6**	**7**	**8**	**9**	**10**	**11**	**12**	**13**
Formula	$C_{20}H_{10}Cu_3N_2O_{10}$	$C_{27}H_{19}Cu_3NO_{12}$	$C_{30}H_{22}CuN_2O_4$	$C_{16}H_{10}Cu_3O_{12}$	$C_{20}H_{14}CoN_2O_5$	$C_{38}H_{30}Co_3N_4O_{16}$	$C_{19}H_{16}N_2NiO_8$	$C_{66}H_{42}Cd_5N_6O_{26}$	$C_{19}H_{13}N_2O_6$
FW	628.92	740.05	538.04	584.86	421.26	975.45	459.05	1897.06	365.31
T/K	293(2)	293(2)	293(2)	293(2)	293(2)	293(2)	293(2)	293(2)	293(2)
Space group	*Pban* (no. 50)	$P2_1/n$ (no. 14)	$P\bar{1}$ (no. 2)	$P2_1/c$ (no. 14)	$P\bar{1}$ (no. 2)	$C2/c$ (no. 15)	$P2_1/n$ (no. 14)	$P\bar{1}$ (no. 2)	$C2/c$ (no. 15)
a/Å	6.8274(6)	7.8407(7)	10.193(1)	5.0445(5)	7.767(1)	30.386(5)	11.280(1)	10.769(2)	26.141(3)
b/Å	12.137(1)	32.422(3)	10.911(1)	10.373(1)	9.460(1)	11.058(2)	8.4929(7)	12.832(3)	7.824(1)
c/Å	21.808(2)	10.3554(9)	12.988(1)	15.588(2)	12.542(2)	12.034(2)	19.965(2)	13.313(3)	19.886(2)
α/°	90	90	105.562(2)	90	73.368(2)	90	90	115.80(3)	90
β/°	90	106.372(2)	111.228(2)	92.152(2)	84.736(2)	100.592(3)	102.315(2)	100.81(3)	126.979(2)
γ/°	90	90	100.438(2)	90	71.367(2)	90	90	90.37(3)	90
V/Å^3	1807.1(3)	2525.7(4)	1233.2(2)	815.1(1)	836.7(2)	3975(1)	1868.7(3)	1618.8(6)	3249.2(7)
Z	4	4	2	4	2	4	4	1	8
D_c/g cm^{-3}	2.312	1.946	1.449	2.383	1.672	1.630	1.632	1.946	1.494
R_{int}	0.0346	0.0273	0.0470	0.0168	0.0161	0.0419	0.0448	0.0321	0.0202
μ/mm^{-1}	3.573	2.577	0.926	3.955	1.064	1.317	1.091	1.708	0.113
Data collected/unique	8903/1772	14 972/5469	8927/4298	3100/1546	6379/3257	13 295/3415	9958/4051	6376/6363	8254/3489
R_1 ($> 2\sigma(I)$/all data)[a]	0.0420/0.0437	0.0488/0.0570	0.0682/0.1016	0.0286/0.0315	0.0404/0.0452	0.0874/0.0925	0.0404/0.0443	0.0576/0.0766	0.0517/0.0598
wR_2 ($> 2\sigma(I)$/all data)[a]	0.1263/0.1278	0.1241/0.1291	0.1603/0.1784	0.0784/0.0805	0.1091/0.1117	0.2353/0.2387	0.1104/0.1133	0.1490/0.1635	0.1373/0.1551
GOF	1.069	1.035	1.068	1.006	1.050	1.047	1.039	1.034	1.090
Residues (e Å^{-3})	–0.577/1.430	–0.379/0.573	–0.481/0.923	–0.433/0.458	–0.659/0.572	–0.606/2.957	–0.447/0.887	–2.788/1.677	–0.356/0.468
CCDC no.	701820	701821	701822	FODHIQ(01)	701824	701825	701826	701827	701828

[a] $R_1 = \sum\|F_o| - |F_c\|/\sum|F_o|$, $wR_2 = [\sum w(F_o^2 - F_c^2)^2/\sum w(F_o^2)^2]^{1/2}$, $w = [\sigma^2(F_o)^2 + (0.1(\max(0, F_o^2) + 2F_c^2)/3)^2]^{-1}$.

Table 3 Selected bond lengths (Å) and bond angles (°) for **5**–**12**

5[a]							
Cu(1)–O(2)	1.911(3)	Cu(1)–O(3)	1.946(3)	Cu(2)–N(1)	2.032(6)	Cu(2)–O(5)	1.998(4)
Cu(1)–O(4)[a]	1.924(4)	Cu(1)–O(1)[b]	2.276(4)	Cu(2)–O(4)	2.368(4)	O(2)–Cu(1)–O(1)[b]	87.5(2)
Cu(1)–O(3)[a]	1.930(3)	Cu(2)–N(2)[d]	2.027(6)	O(2)–Cu(1)–O(4)[a]	95.2(2)	O(4)[a]–Cu(1)–O(1)[b]	89.1(1)
O(2)–Cu(1)–O(3)[a]	165.6(2)	O(3)[a]–Cu(1)–O(1)[b]	105.6(2)	O(5)[c]–Cu(2)–O(4)	121.1(1)	O(5)–Cu(2)–N(1)	88.94(9)
O(4)[a]–Cu(1)–O(3)[a]	91.1(1)	O(3)–Cu(1)–O(1)[b]	103.9(1)	N(2)[d]–Cu(2)–O(4)	90.03(8)	N(2)[d]–Cu(2)–N(1)	180.00(0)
O(2)–Cu(1)–O(3)	91.7(1)	O(3)[a]–Cu(1)–O(3)	79.5(1)	N(1)–Cu(2)–O(4)[c]	89.97(8)	O(5)–Cu(2)–O(5)[c]	177.9(2)
O(4)[a]–Cu(1)–O(3)	165.6(1)	O(4)–Cu(2)–O(4)[c]	179.9(2)	O(5)–Cu(2)–O(4)	58.9(1)	O(5)–Cu(2)–N(2)[d]	91.06(9)
6[a]							
Cu(1)–O(2)	1.892(3)	Cu(1)–O(5)[a]	2.369(3)	Cu(2)–O(4)	1.890(3)	Cu(3)–N(1)	1.994(4)
Cu(1)–O(7)	1.909(3)	Cu(2)–O(6)	1.921(2)	Cu(3)–O(8)	2.399(3)	Cu(3)–O(10)[b]	2.020(3)
Cu(1)–O(6)	1.922(3)	Cu(2)–O(9)	1.865(3)	Cu(3)–O(7)	2.241(3)	Cu(3)–O(2w)	2.148(3)
Cu(1)–O(1)	1.925(2)	Cu(2)–O(1)	1.900(3)	Cu(3)–O(1w)	1.932(3)		
O(2)–Cu(1)–O(7)	95.5(1)	O(1)–Cu(1)–O(5)[a]	88.9(11)	O(10)[b]–Cu(3)–O(7)	152.8(1)	O(2w)–Cu(3)–O(7)	87.7(1)
O(2)–Cu(1)–O(6)	162.1(1)	O(6)–Cu(1)–O(5)[a]	101.2(1)	O(1w)–Cu(3)–N(1)	175.9(2)	O(1w)–Cu(3)–O(8)	92.9(2)
O(7)–Cu(1)–O(6)	92.7(1)	O(9)–Cu(2)–O(6)	93.0(1)	O(2w)–Cu(3)–O(8)	142.9(1)	N(1)–Cu(3)–O(2w)	91.8(1)
O(2)–Cu(1)–O(1)	91.7(1)	O(4)–Cu(2)–O(6)	171.2(1)	O(7)–Cu(3)–O(8)	55.73(9)	O(10)[b]–Cu(3)–O(2w)	119.5(1)
O(7)–Cu(1)–O(1)	171.3(1)	O(9)–Cu(2)–O(4)	93.3(1)	N(1)–Cu(3)–O(7)	91.6(1)	N(1)–Cu(3)–O(8)	83.9(1)
O(6)–Cu(1)–O(1)	79.0(1)	O(9)–Cu(2)–O(1)	172.6(1)	O(1w)–Cu(3)–O(7)	88.6(1)	N(1)–Cu(3)–O(10)[b]	89.8(1)
O(2)–Cu(1)–O(5)[a]	93.8(1)	O(4)–Cu(2)–O(1)	93.9(1)	O(1w)–Cu(3)–O(2w)	92.3(2)		
O(7)–Cu(1)–O(5)[a]	95.5(1)	O(1)–Cu(2)–O(6)	79. 7(1)	O(10)[b]–Cu(3)–O(8)	97.4(1)		
7[a]							
Cu(1)–O(4)[a]	1.937(4)	Cu(1)–O(1)	1.978(4)	Cu(1)–O(3)[b]	2.268(4)	Cu(1)–N(2)	2.042(4)
Cu(1)–N(1)	2.005(5)	Cu(1)–O(2)	2.714(4)	O(1)–Cu(1)–N(1)	93.2(2)	N(1)–Cu(1)–N(2)	173.0(2)
O(4)[a]–Cu(1)–O(1)	159.6(2)	O(4)[a]–Cu(1)–N(2)	86.9(2)	N(2)–Cu(1)–O(3)[b]	90.3(2)	O(4)[a]–Cu(1)–O(3)[b]	111.1(2)
O(4)[a]–Cu(1)–N(1)	89.2(2)	N(1)–Cu(1)–O(3)[b]	96.5(2)	O(1)–Cu(1)–N(2)	88.4(2)		
8[a]							
Cu(1)–O(4)[a]	1.880(2)	Cu(1)–O(1)	1.930(2)	Cu(2)–O(2)	2.244(2)	Cu(2)–O(3)	2.088(2)
Cu(1)–O(2)	1.904(2)	Cu(1)–O(1)[a]	1.914(2)	Cu(2)–O(1w)	1.967(2)		
O(4)[a]–Cu(1)–O(2)	94.29(9)	O(4)[a]–Cu(1)–O(1)	172.09(9)	O(1w)[b]–Cu(2)–O(1w)	180.0(1)	O(3)[b]–Cu(2)–O(3)	180.0
O(4)[a]–Cu(1)–O(1)[a]	94.20(9)	O(1)[a]–Cu(1)–O(1)	79.37(9)	O(1w)–Cu(2)–O(3)	88.78(9)	O(3)–Cu(2)–O(2)	59.76(7)
O(2)–Cu(1)–O(1)[a]	168.02(9)	O(2)–Cu(1)–O(1)	91.43(9)	O(1w)–Cu(2)–O(2)	91.80(8)	O(2)–Cu(2)–O(2)[b]	180.0(1)
9[a]							
Co(1)–O(3)[a]	2.030(2)	Co(1)–N(1)	2.121(2)	Co(1)–O(1w)	2.110(2)	Co(1)–O(1)	2.195(2)
Co(1)–N(2)	2.095(2)	Co(1)–O(2)	2.192(2)				
O(3)[a]–Co(1)–N(2)	112.32(8)	N(2)–Co(1)–N(1)	78.93(9)	O(3)[a]–Co(1)–O(2)	155.08(8)	N(2)–Co(1)–O(1)	151.50(8)
O(3)[a]–Co(1)–O(1w)	89.91(8)	O(1w)–Co(1)–N(1)	170.84(8)	N(1)–Co(1)–O(2)	89.69(9)	O(1w)–Co(1)–O(1)	91.41(8)
N(2)–Co(1)–O(1w)	92.63(9)	N(2)–Co(1)–O(2)	92.54(8)	O(2)–Co(1)–O(1)	59.50(8)	N(1)–Co(1)–O(1)	94.36(9)
O(3)[a]–Co(1)–N(1)	96.55(9)	O(1w)–Co(1)–O(2)	87.11(9)	O(3)[a]–Co(1)–O(1)	95.88(8)		
10[a]							
Co(1)–O(3)	2.063(5)	Co(1)–O(5)[a]	2.084(6)	Co(1)–O(1w)	2.185(6)	Co(2)–O(1)	1.979(6)
Co(1)–O(2)[a]	2.075(5)	Co(1)–N(2)	2.146(7)	Co(1)–N(1)	2.110(6)	Co(2)–O(6)[a]	1.975(6)
O(3)–Co(1)–O(2)[a]	174.2(2)	O(5)[a]–Co(1)–N(1)	88.5(2)	O(3)–Co(1)–O(1w)	89.4(2)	O(6)[b]–Co(2)–O(1)[c]	117.3(2)
O(3)–Co(1)–O(5)[a]	87.1(2)	O(3)–Co(1)–N(2)	87.8(2)	O(2)[a]–Co(1)–O(1w)	96.2(2)	O(6)[a]–Co(2)–O(1)[c]	120.9(2)
O(2)[a]–Co(1)–O(5)[a]	87.1(2)	O(2)[a]–Co(1)–N(2)	93.3(2)	O(5)[a]–Co(1)–O(1w)	174.7(2)	O(6)[b]–Co(2)–O(6)[a]	92.1(3)
O(3)–Co(1)–N(1)	87.3(3)	O(5)[a]–Co(1)–N(2)	94.9(2)	N(1)–Co(1)–O(1w)	87.3(3)	O(1)[c]–Co(2)–O(1)	91.2(3)
O(2)[a]–Co(1)–N(1)	91.9(2)	N(1)–Co(1)–N(2)	174.0(3)	N(2)–Co(1)–O(1w)	89.1(3)		
11[a]							
Ni(1)–O(1w)	2.038(2)	Ni(1)–N(1)	2.090(2)	Ni(1)–O(1)	2.068(2)	Ni(1)–N(2)[b]	2.111(2)
Ni(1)–O(2)[a]	2.042(1)	Ni(1)–O(3)	2.106(1)				
O(1w)–Ni(1)–O(2)[a]	96.84(6)	N(1)–Ni(1)–N(2)[b]	177.88(6)	O(2)[a]–Ni(1)–N(1)	93.86(7)	O(2)[a]–Ni(1)–N(2)[b]	86.16(6)
O(1w)–Ni(1)–O(1)	179.28(6)	O(3)–Ni(1)–N(2)[b]	89.20(6)	O(1)–Ni(1)–N(1)	89.71(6)	O(1)–Ni(1)–N(2)[b]	88.18(6)
O(2)[a]–Ni(1)–O(1)	83.34(5)	N(1)–Ni(1)–O(3)	90.61(6)	O(1w)–Ni(1)–O(3)	87.65(7)	O(1)–Ni(1)–O(3)	92.11(6)
O(1w)–Ni(1)–N(1)	90.97(7)	O(1w)–Ni(1)–N(2)[b]	91.14(6)	O(2)[a]–Ni(1)–O(3)	173.60(5)		
12[a]							
Cd(1)–O(2)[a]	2.243(5)	Cd(1)–N(1)	2.355(6)	Cd(2)–O(9)	2.373(5)	Cd(2)–O(4)	2.354(5)
Cd(1)–O(7)	2.314(5)	Cd(1)–O(3)	2.374(5)	Cd(2)–O(10)	2.492(6)	Cd(3)–N(2)[d]	2.372(6)
Cd(1)–O(1)	2.331(5)	Cd(2)–O(5)[b]	2.251(5)	Cd(2)–O(6)[b]	2.571(6)	Cd(3)–O(8)	2.320(5)
Cd(1)–O(9)	2.344(5)	Cd(2)–N(3)	2.276(6)	Cd(2)–O(3)	2.566(5)	Cd(3)–O(1w)	2.336(6)
O(2)[a]–Cd(1)–O(7)	106.9(2)	O(9)–Cd(1)–O(3)	77.4(2)	N(3)–Cd(2)–O(10)	108.0(2)	O(9)–Cd(2)–O(6)[b]	137.7(2)
O(2)[a]–Cd(1)–O(1)	93.3(2)	N(1)–Cd(1)–O(3)	93.3(2)	O(4)–Cd(2)–O(10)	157.1(2)	O(10)–Cd(2)–O(6)[b]	85.3(2)
O(7)–Cd(1)–O(1)	152.9(2)	O(7)–Cd(1)–O(3)	76.8(2)	O(9)–Cd(2)–O(10)	53.4(2)	O(3)–Cd(2)–O(6)[b]	135.7(2)
O(2)[a]–Cd(1)–O(9)	87.8(2)	O(1)–Cd(1)–O(3)	79.2(2)	O(10)–Cd(2)–O(3)	106.3(2)	O(8)[c]–Cd(3)–O(8)	180.00(0)
O(7)–Cd(1)–O(9)	84.4(2)	O(5)[b]–Cd(2)–N(3)	129.5(2)	O(5)[b]–Cd(2)–O(3)	83.0(2)	O(8)–Cd(3)–O(1w)	85.2(2)
O(1)–Cd(1)–O(9)	78.3(2)	O(5)[b]–Cd(2)–O(4)	94.7(2)	N(3)–Cd(2)–O(3)	129.8(2)	O(1w)–Cd(3)–O(1w)[c]	180.0(3)
O(2)[a]–Cd(1)–N(1)	101.3(2)	N(3)–Cd(2)–O(4)	82.9(2)	O(4)–Cd(2)–O(3)	53.7(2)	O(8)[c]–Cd(3)–N(2)[d]	89.5(2)
O(7)–Cd(1)–N(1)	95.2(2)	O(5)[b]–Cd(2)–O(9)	128.8(2)	O(9)–Cd(2)–O(3)	73.2(2)	O(1w)–Cd(3)–N(2)[d]	86.6(2)
O(1)–Cd(1)–N(1)	98.4(2)	N(3)–Cd(2)–O(9)	99.8(2)	N(3)–Cd(2)–O(6)[b]	82.8(2)	N(2)[d]–Cd(3)–N(2)[e]	180.00(0)
O(9)–Cd(1)–N(1)	170.5(2)	O(4)–Cd(2)–O(9)	105.7(2)	O(4)–Cd(2)–O(6)[b]	116.6(2)		
O(2)[a]–Cd(1)–O(3)	164.5(2)	O(5)[b]–Cd(2)–O(10)	93.5(2)	O(5)[b]–Cd(2)–O(6)[b]	53.3(2)		

[a] Symmetry codes. For **5**: [a] $-x, -y+1, -z+1$; [b] $x+1/2, -y+3/2, z$; [c] $x, -y+1, -z+3/2$; [d] $x+1, y, z$. For **6**: [a] $-x+1, -y, -z+1$; [b] $x, y, z-1$. For **7**: [a] $x+1, y, z$; [b] $-x+1, -y+1, -z+1$. For **8**: [a] $-x-2, -y, -z$; [b] $-x-2, -y+1, -z$. For **9**: [a], $x-1, y+1, z$. For **10**: [a] $x, -y+1, z-1/2$; [b] $-x+1, -y+1, -z$; [c] $-x+1, y, -z-1/2$; [d] $x, -y+1, z+1/2$; [e] $-x+1, -y+2, -z-1$; [f] $-x+1/2, -y+1/2, -z-1$. For **11**: [a] $-x+5/2, y+1/2, -z+5/2$; [b] $x-1, y, z$. For **12**: [a] $-x+1, -y, -z-2$; [b] $-x+1, -y+1, -z-2$; [c] $-x, -y+1, -z-2$; [d] $-x, -y, -z-3$; [e] $x, y+1, z+1$; [f] $x, y-1, z-1$; [g] $-x+2, -y+1, -z-1$.

atoms were generated geometrically at a C–H distance of 0.96 Å. Data collection and structural refinement parameters are given in Table 2 and selected bond distances and angles are given in Table 3.

Magnetic measurements

Magnetic susceptibility measurements have been carried out on a Quantum Design MPMS-XL7 SQUID magnetometer between 1.8–300 K and ±70 KOe. Diamagnetic correction was calculated from Pascal constants and applied to the observed magnetic susceptibilities.

Acknowledgements

This work was supported by the "973 Project" (2007CB815302 & 2007CB815305) and NSFC (20821001 & 20525102). The authors thank Prof. Marc Drillon (IPCMS, 23 rue du Loess, B.P. 43, 67034 Strasbourg Cedex 2 France) for helpful discussions.

Notes and references

1 (*a*) X.-M. Chen and M.-L. Tong, *Acc. Chem. Rev.*, 2007, **40**, 162; (*b*) X.-M. Zhang, *Coord. Chem. Rev.*, 2005, **249**, 1201.
2 C.-M. Liu, S. Gao and H.-Z. Kou, *Chem. Commun.*, 2001, 1670.
3 (*a*) X.-M. Zhang, M.-L. Tong and X.-M. Chen, *Angew. Chem., Int. Ed.*, 2002, **41**, 1029; (*b*) X.-M. Zhang, M.-L. Tong, M.-L. Gong, H.-K. Lee, L. Luo, K.-F. Li, Y.-X. Tong and X.-M. Chen, *Chem.–Eur. J.*, 2002, **8**, 3187.
4 (*a*) J. Tao, Y. Zhang, M.-L. Tong, X.-M. Chen, T. Yuen, C.-L. Lin, X.-Y. Huang and J. Li, *Chem. Commun.*, 2002, 1342; (*b*) Y.-Z. Zheng, M.-L. Tong and X.-M. Chen, *New J. Chem.*, 2004, **28**, 1412; (*c*) Y.-Z. Zheng, M.-L. Tong and X.-M. Chen, *J. Mol. Struct.*, 2006, **796**, 9; (*d*) M.-H. Zeng, W.-X. Zhang and X.-M. Chen, *Dalton Trans.*, 2006, 5294; (*e*) H. Sheng, J.-C. Chen, M.-L. Tong, B. Wang, Y.-Y. Xing and S. R. Batten, *Angew. Chem., Int. Ed.*, 2005, **44**, 5471.
5 (*a*) J.-P. Zhang, S.-L. Zheng, X-C. Huang and X-M. Chen, *Angew. Chem., Int. Ed.*, 2004, **43**, 206; (*b*) J.-P. Zhang, Y.-Y. Lin, H.-C. Huang and X.-M. Chen, *J. Am. Chem. Soc.*, 2005, **127**, 5495; (*c*) L. Cheng, W.-X. Zhang, B.-H. Ye, J.-B. Lin and X.-M. Chen, *Inorg. Chem.*, **46**, 1135; (*d*) R.-G. Xiong, X. Xue, H. Zhao, X.-Z. You, B. F. Abrahams and Z.-L. Xue, *Angew. Chem., Int. Ed.*, 2002, **114**, 3800.
6 (*a*) D. Li, T. Wu, X.-P. Zhou, R. Zhou and X.-C. Huang, *Angew. Chem., Int. Ed.*, 2005, **44**, 4175; (*b*) X.-M. Zhang, R.-Q. Fang and H.-S. Wu, *J. Am. Chem. Soc.*, 2005, **127**, 7670; (*c*) J. Wang, S.-L. Zheng, S. Hu, Y.-H. Zhang and M.-L. Tong, *Inorg. Chem.*, 2007, **46**, 795; (*d*) N. Zheng, X. Bu and P. Feng, *J. Am. Chem. Soc.*, 2002, **124**, 9688.
7 (*a*) X.-C. Huang, J.-P. Zhang, Y.-Y. Lin and X.-M. Chen, *Chem. Commun.*, 2004, 1100; (*b*) Y.-Z. Zheng, W. Xue, M.-L Tong, W.-X. Zhang, X.-M. Chen, F. Grandjean and G. J. Long, *Inorg. Chem.*, 2008, **47**, 4077.
8 S.-L. Zheng, J.-P. Zhang, W.-T. Wong and X.-M. Chen, *J. Am. Chem. Soc.*, 2003, **125**, 6882.
9 (*a*) C. N. R. Rao, S. Natarajan and R. Vaidhyanathan, *Angew. Chem., Int. Ed.*, 2004, **43**, 1466; (*b*) S. Kitagawa, R. Kitaura and S.-I. Noro, *Angew. Chem., Int. Ed.*, 2004, **43**, 2334; (*c*) C. Janiak, *Dalton Trans.*, 2003, 2781.
10 (*a*) Y.-Z. Zheng, M.-L. Tong, W.-X. Zhang and X.-M. Chen, *Angew. Chem., Int. Ed.*, 2006, **45**, 6310; (*b*) Y.-Z. Zheng, M.-L. Tong, W. Xue, W.-X. Zhang, X.-M. Chen, F. Grandjean and G. J. Long, *Angew. Chem., Int. Ed.*, 2007, **46**, 6076; (*c*) Y.-Z. Zheng, W. Xue, S.-L. Zheng, M.-L. Tong and X.-M. Chen, *Adv. Mater.*, 2008, **20**, 1534; (*d*) Y.-Z. Zheng, M.-L. Tong, W.-X. Zhang and X.-M. Chen, *Chem. Commun.*, 2006, 165; (*e*) Y.-Z. Zheng, W. Xue, W.-X. Zhang, M.-L. Tong and X.-M. Chen, *Inorg. Chem.*, 2007, **46**, 6437; (*f*) Y.-Z. Zheng, W. Xue, M.-L. Tong, X.-M. Chen and S.-L. Zheng, *Inorg. Chem.*, 2008, **47**, 11202.
11 C. Coulon, H. Miyasaka and R. Clérac, *Struct. Bonding (Berlin)*, 2006, **122**, 163.
12 E. C. Constable, *Metals and Ligand Reactivity*, VCH, Weinheim, 1996.
13 (*a*) S.-Y. Yang, L.-S. Long, R.-B. Huang, L.-S. Zheng and S.-W. Ng, *Inorg. Chim. Acta*, 2005, **358**, 1882; (*b*) Y.-Q. Jiang, Z.-H. Zhou and Z.-B. Wei, *Chin. J. Struct. Chem.*, 2005, **24**, 457.
14 (*a*) O. Kahn, *Molecular Magnetism*, VCH, New York, 1993; (*b*) C. L. Carlin, *Magnetochemistry*, Springer, Berlin, 1986.
15 A. Bencini, C. Benelli, A. Dei and D. Gatteschi, *Inorg. Chem.*, 1985, **24**, 695.
16 V. H. Crawford, H. W. Richardson, J. R. Wasson, D. J. Hodgson and W. E. Hatfield, *Inorg. Chem.*, 1976, **15**, 2107.
17 (*a*) M. Drillon, E. Coronado, M. Belaiche, R. L. Carlin, *J. Appl. Phys.* 1988, 63, 3551; (*b*) R. Georges, J. J. Borrás-Almenar, E. Coronado, J. Curély, M. Drillon, One-dimensional Magnetism: An Overview of the Models in *Magnetism: Molecules to Materials*, ed. J. S. Miller and M. Drillon, Wiley, Germany, 2001, vol. I, p. 1.
18 (*a*) C. Qin, X.-L. Wang, Y.-G. Li, E.-B. Wang, Z.-M. Su, L. Xu and R. Clérac, *Dalton Trans.*, 2005, 2609; (*b*) P. S. Mukherjee, S. Konar, E. Zangrando, T. Mallah, J. Ribas and N. R. Chaudhuri, *Inorg. Chem.*, 2003, **42**, 2695; (*c*) M. Du, X.-H. Bu, Y.-M. Guo, L. Zhang, D.-Z. Liao and J. Ribas, *Chem. Commun.*, 2002, 1478; (*d*) A. J. Costa-Filho, O. R. Nascimento, L. Ghivelder and R. Calvo, *J. Phys. Chem. B*, 2001, **105**, 5039; (*e*) J. Sanchiz, Y. Rodruez-Martín, C. Ruiz-Pérez, A. Mederos, F. Lloret and M. Julve, *New J. Chem.*, 2002, **26**, 1624; (*f*) J.-M. Rueff, S. Pillet, N. Claiser, G. Bonaventure, M. Souhassou and P. Rabu, *Eur. J. Inorg. Chem.*, 2002, 895.
19 M. E. Fisher, *Am. J. Phys.*, 1964, **32**, 343.
20 (*a*) A. Fu, X. Huang, J. Li, T. Yuen and C. L. Lin, *Chem.–Eur. J.*, 2002, **8**, 2239; (*b*) X.-Y. Wang, L. Wang, Z.-M. Wang, G. Su and S. Gao, *Chem. Mater.*, 2005, **17**, 6369; (*c*) E.-Q. Gao, Z.-M. Wang and C.-H. Yan, *Chem. Commun.*, 2003, 1748.
21 S. Chikazumi, *Physics of Ferromagnetism*, Clarendon Press, Oxford Science Publications, Oxford, 1997p. 521.
22 (*a*) P. M. Richards, *Phys. Rev. B: Condens. Matter Mater. Phys.*, 1974, **10**, 4687; (*b*) P. Panissod, M. Drillon, in *Magnetism: Molecules to Materials*, ed. J. S. Miller and M. Drillon, Wiley-VCH Verlag, Berlin, 2001, vol. IV, pp. 234–270; (*c*) J. Souletie, P. Rabu, M. Drillon, in *Magnetism: Molecules to Materials*, ed. J. S. Miller and M. Drillon, Wiley-VCH Verlag, Berlin, 2005, vol. V, pp. 347–377.
23 G. M. Sheldrick, *SADABS, Program for area detector adsorption correction*, Institute for Inorganic Chemistry, University of Göttingen, Germany, 1996.
24 G. M. Sheldrick, *SHELXL-97, Program for refinement of crystal structures*, University of Göttingen, Germany, 1997.
25 *SHELXTL 6.10*, Bruker Analytical Instrumentation, Madison, Wisconsin, USA, 2000.

